Modular Topology Optimization of a Humanoid Arm

Lukas Krischer
Laboratory for Product Development and Lightweight Design
Technical University of Munich
Garching, Germany
Email: lukas.krischer@tum.de

Anand Vazhapilli Sureshbabu
Laboratory for Product Development and Lightweight Design
Technical University of Munich
Garching, Germany
Email: anand.suresh@tum.de

Markus Zimmermann
Laboratory for Product Development and Lightweight Design
Technical University of Munich
Garching 85748, Germany
Email: zimmermann@tum.de

***Abstract*—The development of humanoid robots is typically driven by control, kinematics and actuator design, often resulting in unnecessarily heavy structural components. Topology optimization can be used to reduce weight. Unfortunately, monolithic topology optimization is numerically expensive for a multi-component robot system that assumes different poses. It becomes even more expensive when optimal materials are to be selected for each segment. This paper proposes a top-down approach where components of the robot are optimized separately. In the first step, requirements on the stiffness of the entire structure for different poses are decomposed into precise displacement constraints for each component without any assumption related to geometry or material. In the second step, these constraints are used for topology optimization of the individual components for each possible material. The approach is applied to a two-segment humanoid arm for ABS, aluminum and titanium. The resulting design, obtained at moderate cost, satisfies all stiffness requirements for all poses considered.**

I. Introduction

In humanoid robotics, lightweight design plays a significant role due to limited energy storage capacity and collision safety in human interaction applications. However, existing lightweight robots often focus only on control, kinematics and actuator design rather than the optimization of the mechanical support structure. For example, Schäffler et al. [1] developed the DLR lightweight robot, in which low mass was realized via a lightweight actuation with harmonic drive gears and high density motors. Buchler et al. [2] placed the actuators of a robot arm in the base instead of the moving links in order to reduce the weight of the moving masses. Mori et al. [3] designed a humanoid robot arm, where the lightweight design was achieved by a cable-driven architecture with integrated low weight compressors in the arm links.

Numerical optimization can be used to derive customized lightweight support structures. Topology optimization, first introduced by Bendsøe and Sigmund [4], offers the largest design freedom among the existing methods and hence provides the biggest potential of mass reduction. However, the high computational costs of structural optimization methods especially in the field of robotics, where multiple components and time-varying kinematic configurations are involved, makes their application difficult.

One way of reducing the computational cost is to solve the problem only for specific static robot configurations. Albers et al. [5] employed a static topology optimization for a thorax, Kwon et al. [6] optimized the lower body of a biped humanoid and Junk et al. [7] the pelvis of a robot. Further, Huang and Zhang [8] carried out a static topology optimization of an industrial robot with loads of a flexible multi body simulation, whereas Yunfei et al. [9] optimized a robot upper arm with respect to representative static load cases and considered dynamic behavior by constraining the eigenfrequencies of the structure. However, in none of the before-mentioned works a system was optimized, but only single components.

In system optimization, monolithic and distributed architectures are typically distinguished. In monolithic structures a single design problem is solved [10]. For instance, Zhou and Saitou [11] carried out a multi-component topology optimization, where the single components of a system were optimized with respect to the system compliance subject to manufacturing constraint. However, for large design problems, monolithic architectures often exceed computational capacities. In contrast, distributed architectures decompose the problem into smaller sub-problems containing subsets of the variables and constraints. Most of those architectures maintain a certain coupling of the design variables, system responses or constraints in order to guarantee consistency of the system [10]. For instance, analytical target cascading developed by Kim et al. [12] propagates system requirements down to the components as precise target values, requiring coordinate strategies when requirements cannot be satisfied.

In the context of lightweight design, not only the geometrical topology Ω, but also the used materials are of special interest. For a limited design space, the material with the highest stiffness-density ratio E/ρ is often not mass optimal. Therefore, also several material combinations are to be considered. The combinatorics of this modularity adds additional computational costs to the problem, also for classical distributed optimization architectures. These combinatorics can be treated by component-wise optimization, where consistency is ensured once at the system level and afterwards each sub-problem can be solved completely independently of each other. For a robot arm consisting of $k{=}2$ components with n

DoF each, m=3 different materials and d=5 considered static poses, a basic Gauß-Jordan elimination, for instance, has the computational complexity of $\mathcal{O}(\sim n^3)$ [13]. One analysis of a system with a monolithic or classical distributed architecture is factor 320 ($d\ k^m(kn)^3$=$320n^3$) times more expansive than a single component analysis. A complete decoupled procedure in comparison only takes 6 times longer ($km(n)^3$=$6n^3$). Depending on the utilized solving algorithm, a time improvement up to factor 53.3 is possible.

This motivates the need for a modular optimization scheme enabling independent component optimization. Kim et al. [14] carried out an internal energy minimization with a full decoupling of the structures on the system level utilizing a regression model for the mass estimation. A component-wise topology optimization was carried out afterwards based on the allocated mass limits. Although, internal energy is the classical optimization objective in topology optimization, its condensed scalar representation does not allow for precise assessment with respect to the deformation behavior of a component. Quantitative requirements concerned with displacement values cannot be investigated within this formulation. Further, Wang et al. [15] conducted a stiffness optimization based on a parametrization of a topology. Here, the detailed structures were parametrized before the system optimization was conducted, arguing that the changes in the design do not undergo significant changes afterwards. However, this premature determination of a specific topology limits the design freedom and hence the lightweight potential, because the consecutive component-wise optimization just adjusts the parametrized geometry.

The objective of this paper is to carry out a modular optimization of the two segments with respect to displacement requirements for three different materials. Modular refers in this context to a separate optimization with appropriate boundary conditions. Utilizing topology optimization, maximum design freedom is provided, while displacement constraints ensure the required system properties.

II. Problem Setup

The overall development goal is to design an additive manufactured lightweight humanoid robot arm. Two requirements were formulated concerning the structural design:

(1) The robot arm must hold a weight of 1kg at any position with an maximum end effector displacement of d_0=1mm.
(2) The arm geometry is based on measurements of a 50th percentile male [16].

The robot arm has four DoF (cf. Fig. 1), with the shoulder realized by three sequential revolute joints for the pitch (θ_1), roll (θ_2) and yaw (θ_3) movement. The lower arm possesses the remaining elbow flexion (θ_4) DoF, whereas the wrist of the arm is fixed. A position control strategy for the individual joint angles is utilized, under the assumption of a perfect actuation, i.e. instant response capability and unbounded force capacity. The classical DH parameters as well as the corresponding ranges of motion are shown in Table I. To calculate the end

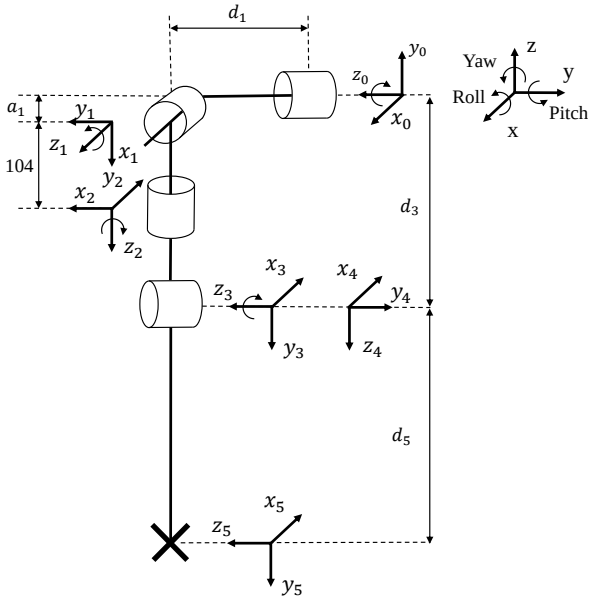

Fig. 1: Kinematic model of the robot arm with three subsequent joints for the shoulder movement (1,2 and 3), the elbow flexion (4) and the fixed wrist joint (5).

TABLE I: DH-Parameters $[\theta_j, d_j, a_j, \alpha_j]$ and ranges of joint angles θ_j^* for the respective joints j.

j	θ_j (°)	θ_j^* (°)	d_j (mm)	a_j (mm)	α_j (°)
1	$\theta_1^* - 90$	$[-30, 110]$	105	5	90
2	$\theta_2^* + 90$	$[-90, 90]$	0	0	90
3	$\theta_3^* + 90$	$[-90, 10]$	280	0	90
4	θ_4^*	$[0, 130]$	0	0	-90
5	0	-	300	0	90

effector positions, the transformation matrices for the forward kinematics are then defined as:

$$ {}^{j-1}\boldsymbol{T}_j = \begin{bmatrix} c\theta & -s\theta\ c\alpha & st\ s\alpha & a\ c\theta \\ s\theta & c\theta\ c\alpha & -ct\ s\alpha & a\ s\theta \\ 0 & s\alpha & c\alpha & d \\ 0 & 0 & 0 & 1 \end{bmatrix} \tag{1} $$

$$ {}^0\boldsymbol{T}_5 = {}^0\boldsymbol{T}_1\,{}^1\boldsymbol{T}_2\,{}^2\boldsymbol{T}_3\,{}^3\boldsymbol{T}_4\,{}^4\boldsymbol{T}_5 \tag{2} $$

with $c\theta$=$cos(\theta_j)$, $s\theta$=$sin(\theta_j)$, $c\alpha$=$cos(\alpha_j)$, $s\alpha$=$sin(\alpha_j)$, a=a_j and d=d_j.

For requirement (1), five representative static load cases were derived: Three worst-case bending poses (1−3.) with different θ_3 angles, one torsional load case for the upper arm (4.) and one normal force pose (5.) (cf. Table II and Fig 3). The design space is defined in accordance to requirement (2) with respect to a 50th percentile male. The joints are only considered as blocker geometries and will be designed later

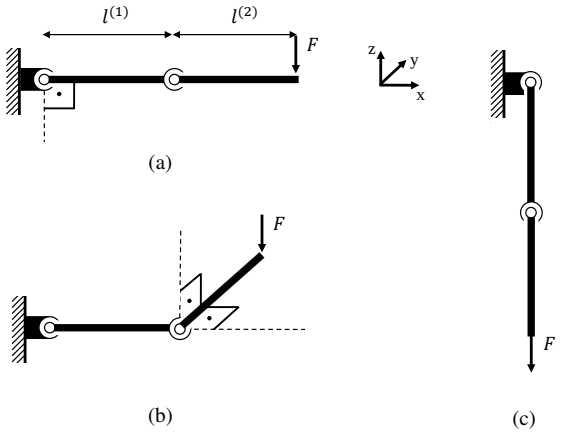

Fig. 2: Representative static load cases of holding a weight of 1kg for (a) 1-3 bending, (b) 4 torsion and (c) 5 normal force

TABLE II: Joint angles θ_j^* of the representative static load cases of requirement (1)

Load Cases	1	2	3	4	5
θ_1^* (°)	90	90	90	90	0
θ_2^* (°)	0	0	0	90	0
θ_3^* (°)	−90	10	−40	−90	0
θ_4^* (°)	0	0	0	90	0

in the design process (see Fig. 3).

A topology optimization procedure is carried out on a geometrically confined design space. Since the resulting designs of a topology optimization do often have complex geometrical features, additive manufacturing is utilized. Three different materials were considered: Acrylnitril-Butadien-Styrol-Copolymere (ABS), a common material for Fused Deposition Modeling (FDM), an Aluminum Alloy (AlSi10MG) and Titanium (Ti64), which both can be used for Selective Laser Melting (SLM).

III. Design Approach

A. Overview

Fig. 4 illustrates the dependencies between the design variables and the resulting deformation measures and masses. The lower and upper arm consist of geometric topologies Ω_k and the material $M_k = [E_m, \rho_m, \nu_m]$. For a given load case pose, $\boldsymbol{\delta}^{(1)}$ and $\boldsymbol{\varphi}^{(1)}$ are quantities whose values will be uniquely determined by properties of component 1 only, i.e. Ω_1 and M_1. Similarly, $\boldsymbol{\delta}^{(2)}$ will be uniquely determiend by Ω_2 and M_2. Therefore, $\boldsymbol{\delta}^{(1)}$, $\boldsymbol{\delta}^{(2)}$ and $\boldsymbol{\varphi}^{(1)}$ can be treated as component properties and used to formulate component requirements.

As a first step, a bottom-up mapping between the corresponding upper and lower arm displacements and the overall displacement is derived. The component requirements are then computed as feasible regions of displacements and rotations

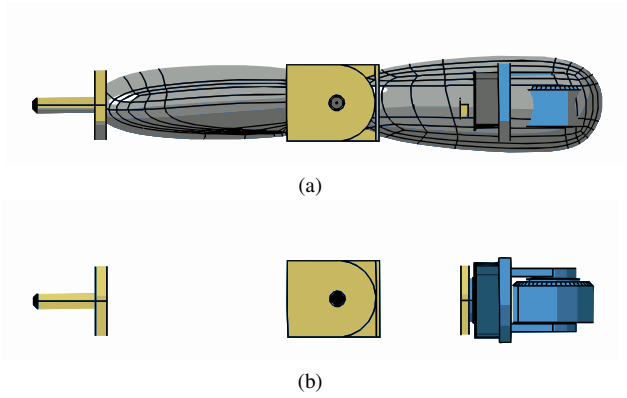

Fig. 3: (a) Design space and (b) blocker joint geometry of the robot arm

for both segments with respect to the given system requirements. The component geometries are optimized for each material using a topology optimization scheme.

B. Requirement Decomposition

The relations between the end effector displacement and the component deformations are illustrated in Fig. 5, where $\boldsymbol{d}^{(1)}$ and $\boldsymbol{d}^{(2)}$ are measured in the assembled system, whereas $\boldsymbol{\delta}^{(1)}$, $\boldsymbol{\delta}^{(2)}$ and $\boldsymbol{\varphi}^{(1)}$ are component quantities. The end effector displacement is given by:

$$\begin{aligned} \boldsymbol{d} &= \boldsymbol{d}^{(1)} + \boldsymbol{d}^{(2)} \\ &= \boldsymbol{\delta}^{(1)} + \boldsymbol{l}^{(2)} \times \boldsymbol{\varphi}^{(1)} + \boldsymbol{\delta}^{(2)}. \end{aligned} \tag{3}$$

The displacements $\boldsymbol{\delta}^{(k)}$ and the rotations $\boldsymbol{\varphi}^{(1)}$ are calculated from the respective local displacements of the lower and upper arm. Therefore, they need to be transformed to the global coordinate system in order to calculate the end effector displacement by:

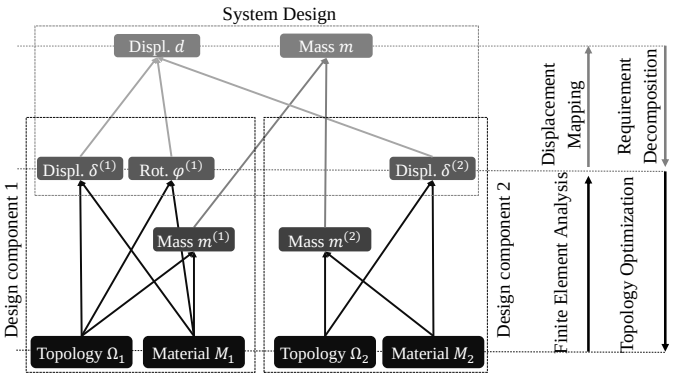

Fig. 4: Dependency graph of the quantities of interest (top) and the design variables (bottom) and the corresponding bottom-up and top-down mappings (right)

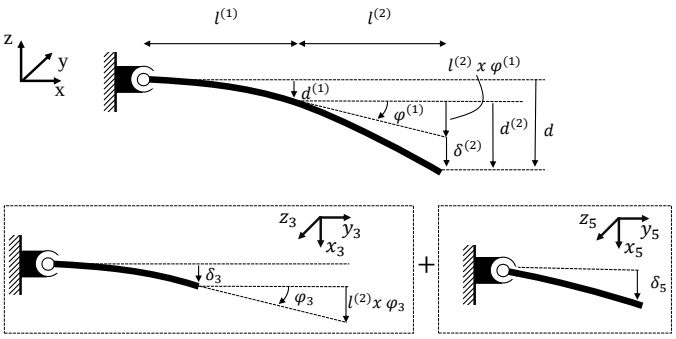

Fig. 5: System assembly (top) and isolated components (bottom) illustrating the relation between end effector displacement d and the corresponding deformations $\boldsymbol{\delta}^{(k)}$, $\varphi^{(1)}$

$$\begin{bmatrix} \delta_x^{(1)} \\ \delta_y^{(1)} \\ \delta_z^{(1)} \\ 0 \end{bmatrix} = {}^0\boldsymbol{T}_1\,{}^1\boldsymbol{T}_2\,{}^2\boldsymbol{T}_3 \begin{bmatrix} \delta_{3x} \\ \delta_{3y} \\ \delta_{3z} \\ 0 \end{bmatrix} \tag{4}$$

$$\begin{bmatrix} \varphi_x^{(1)} \\ \varphi_y^{(1)} \\ \varphi_z^{(1)} \\ 0 \end{bmatrix} = {}^0\boldsymbol{T}_1\,{}^1\boldsymbol{T}_2\,{}^2\boldsymbol{T}_3 \begin{bmatrix} \varphi_{3x} \\ \varphi_{3y} \\ \varphi_{3z} \\ 0 \end{bmatrix} \tag{5}$$

$$\begin{bmatrix} \delta_x^{(2)} \\ \delta_y^{(2)} \\ \delta_z^{(2)} \\ 0 \end{bmatrix} = {}^0\boldsymbol{T}_1\,{}^1\boldsymbol{T}_2\,{}^2\boldsymbol{T}_3\,{}^3\boldsymbol{T}_4\,{}^4\boldsymbol{T}_5 \begin{bmatrix} \delta_{5x} \\ \delta_{5y} \\ \delta_{5z} \\ 0 \end{bmatrix} \tag{6}$$

The decoupling of the tip displacement $\boldsymbol{d}$ is accomplished by allocating a certain stiffness budget to the lower arm and upper arm displacements. Note, that we treat stiffness as the inverse of displacement for a given load. It must be ensured that the system quantity does not violate requirement (1), i.e.,

$$|\boldsymbol{d}| \leq d_0, \tag{7}$$

with $\boldsymbol{d} = \boldsymbol{\delta}^{(1)} + \boldsymbol{l}^{(2)} \times \boldsymbol{\varphi}^{(1)} + \boldsymbol{\delta}^{(2)}$. This is satisfied when

$$|\boldsymbol{\delta}^{(1)} + \boldsymbol{l}^{(2)} \times \boldsymbol{\varphi}^{(1)}| \leq \alpha d_0 \tag{8}$$

$$|\boldsymbol{\delta}^{(2)}| \leq (1-\alpha)\, d_0. \tag{9}$$

as (8) and (9) include only properties of component 1 and 2, respectively, they server as component requirements. The stiffness budget distribution $\alpha \in [0, 1]$ provides an improtant bounday condition for component optimization. In a pure top-down approach, it cannot be computed from the available information. Therefore it set to be $\alpha = 3/4$, motivated by the reference structure in Appendix A.

This kind of quantitative top-down design was introduced by Zimmermann and Hoessle [18] and embedded into a design procedure in [17]. Based on system requirements, so-called solution spaces are computed representing sets of good designs. The edges of box-shaped solution spaces are permissible intervals for component properties and can be used to formulate component requirements. This was later generalized to so-called component solution spaces in [19] without restriction to particular shapes, however, restricted to performance functions that are additively decomposable. The approach presented here is a further extension of it, as $|\boldsymbol{d}|$ is not additively decomposable into component properties.

C. Topology Optimization

The optimization problem for the upper arm can be formulated as

$$\begin{aligned} &\min_{\rho_e} m^{(1)}(\rho_e(\boldsymbol{x})) \\ \text{s.t. : } &|\boldsymbol{\delta}^{(1,c)} + \boldsymbol{l}^{(2,c)} \times \boldsymbol{\varphi}^{(1,c)}| - \alpha d_0 \leq 0 \\ &\left(\sum_{e=1}^{i^{(1)}} \rho_e^p \boldsymbol{K}_e \right) \boldsymbol{D}^{(1,c)} - \boldsymbol{F}^{(1,c)} = 0 \\ &0 < \rho_e \leq 1 \qquad \text{for } c{=}1,..,5 \end{aligned} \tag{10}$$

where five load cases are considered for the displacement constraints and the finite element model with $\boldsymbol{D}^{(1,c)}$ as the displacement vector, $\boldsymbol{F}^{(1,c)}$ as the load vector, $\boldsymbol{K}_e$ as the local stiffness matrix and ρ_e for the element density. The optimization problem for the lower arm reads

$$\begin{aligned} &\min_{\rho_e} m^{(2)}(\rho_e(\boldsymbol{x})) \\ \text{s. t.: } &|\boldsymbol{\delta}^{(2,c)}| - (1-\alpha) d_0 \leq 0 \\ &\left(\sum_{e=1}^{i^{(2)}} \rho_e^p \boldsymbol{K}_e \right) \boldsymbol{D}^{(2,c)} - \boldsymbol{F}^{(2,c)} = 0 \\ &0 < \rho_e \leq 1 \qquad \text{for } c{=}1,..,5 \end{aligned} \tag{11}$$

with $\boldsymbol{D}^{(2,c)}$ and $\boldsymbol{F}^{(2,c)}$ being the displacement vector and force vector of the finite element model of the lower arm.

To compute the system responses, finite element models for both components were built in Altair OptiStruct 2017.3. A linear elastic material model was utilized with $i^{(1)}{=}157083$ solid elements and $n^{(1)}{=}30272$ nodes for the upper arm and $i^{(2)}{=}251323$ elements and $n^{(2)}{=}46201$ nodes for the lower arm. The yet unknown joint structure was modeled with RBE2 elements (cf. Fig. 6). The material data can be obtained from Table III.

For the topology optimization, the classical Solid Isotropic Material Penalization (SIMP) method [4] was utilized with a dual optimization algorithm based on separate convex optimization. In order to achieve similar convergence behavior for the three different material configurations, two consecutive topology optimization runs were performed with a penalty factor of $p_{(1)} = 4$ for the first and $p_{(2)} = 7$ for the second run. All optimization settings can be seen in Table IV.

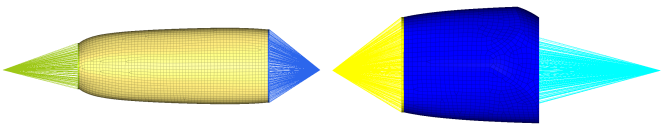

(a) (b)

Fig. 6: Finite element model of the (a) lower and (b) upper arm

TABLE III: Material data

Material	Young's Modulus E (GPa)	Poisson Ratio ν	Density ρ (g/cm^3)
ABS	1.91	0.36	1.07
AlSi10MG	70.0	0.33	2.70
Ti64	160	0.29	8.20

TABLE IV: Topology optimization settings

Max Iterations	200
Initial Fraction ρ_e	0.6
Penalty Factor p	4 / 7
Checkerboard Control	on

IV. Results

Fig. 7 shows the results of the upper arm topology optimization. In the first (a-c) and second row (d-f) are the continuous density fields as the results of the two sequential optimization runs. The third row (g-i) contains a discrete interpretation of the results with a threshold density value of ρ_{th}=0.5. In Table V, the resulting masses as well as the constraint responses of the second topology optimization run are shown. The aluminum concept exhibits the lowest absolute weight of m=49.5g with multiple thin truss-like elements. Titanium, with more distinct but less truss structures, has a slightly greater weight of m=60.1g, whereas the ABS design is the heaviest with m=85.9g. All concepts satisfy the given displacement requirements for the five load cases. In contrast to the bending and torsion load cases, the normal force load case is not active and therefore negligible.

For the lower arm, the results are shown in Fig. 8. The first two rows (a-c) and (d-f) show the results of the first and second topology optimization run. For the last row (g-i) a threshold value of $\rho_{th} = 0.5$ was applied for the geometrical identification of the main features of the respective topologies. Again, the final ABS topology contains continuous regions of materials, in contrast to the aluminum and titanium concepts, where discrete truss-like structures are obtained. The results of the final topology optimization run can be seen in Table VI. The aluminum structure performed the best with a weight of $m = 56.1$g. Then titanium with $m = 77.9$g follows and the ABS concept with $m = 128$g has the highest weight. For all three lower arm concepts, the constraints of the first four load cases are active, whereas load case five seems to be noncritical.

TABLE V: Initial mass m_0, optimized mass m_{opt}, and the resulting deflection for all 5 load cases of the upper arm

	m_0 (g)	m_{opt} (g)	$\lvert\boldsymbol{\delta}^{(1,c)}+\boldsymbol{l}^{(2,c)}\times\boldsymbol{\varphi}^{(1,c)}\rvert \leq 0.75$ (mm)				
			c=1	c=2	c=3	c=4	c=5
ABS	880.6	85.92	0.75	0.75	0.75	0.75	0.012
Al	2222	49.52	0.73	0.73	0.73	0.73	0.022
Ti64	3621	60.13	0.73	0.74	0.74	0.74	0.022

TABLE VI: Initial mass m_0, optimized mass m_{opt}, and the resulting deflection for all 5 load cases of the lower arm

	m_0 (g)	m_{opt} (g)	$\lvert\boldsymbol{\delta}^{(2,c)}\rvert \leq 0.25$ (mm)				
			c=1	c=2	c=3	c=4	c=5
ABS	1375	128.1	0.25	0.25	0.25	0.25	0.015
Al	3475	56.12	0.25	0.25	0.24	0.25	0.019
Ti64	5652	77.92	0.25	0.25	0.25	0.25	0.026

V. Discussion

In general, all material concepts could reduce the weight of the initial design significantly. Aluminum with the highest stiffness-density ratio E/ρ achieved the expected best results. By observing the resulting topologies (cf. Fig 7 and Fig. 8), one can see that the material is mostly gathered at the outer boundaries of the design domain, hence the results are strongly dependent on the chosen design domain.

Furthermore, even though the optimization converged with active constraints, hinting for a mass optimal solution, the continuous density field needs to be transferred to a producible structure. Only discrete density values of ρ_e=1 are physically meaningful and can be manufactured by e.g. additive manufacturing methods. This is a known problem in topology optimization and especially critical for local displacement requirements [20]. Applying a simple threshold, in which the corresponding element densities ρ_e are either turned void or solid, results in too stiff structures. For instance, the lower arm made of aluminum (cf. Fig 8h) is with a realized displacement of $|\delta^{(2)}| = 0.0784$ mm factor 3 stiffer than required. This hints at a remaining potential with respect to lightweight design.

Additionally, a buckling analysis as well as a strength analysis should be carried out for the slender truss associated elements of the aluminum and titanium designs. These constraints are in general difficult to apply in topology optimization because of the high numbers of design variables.

The decoupling itself proved to be computationally efficient, because not only the complexity of the material combinatorics could be reduced, but also the costs of the analysis itself. Since the boundary conditions and therefore the reduced stiffness matrix $\boldsymbol{K}$ in the local coordinate system is the same for all

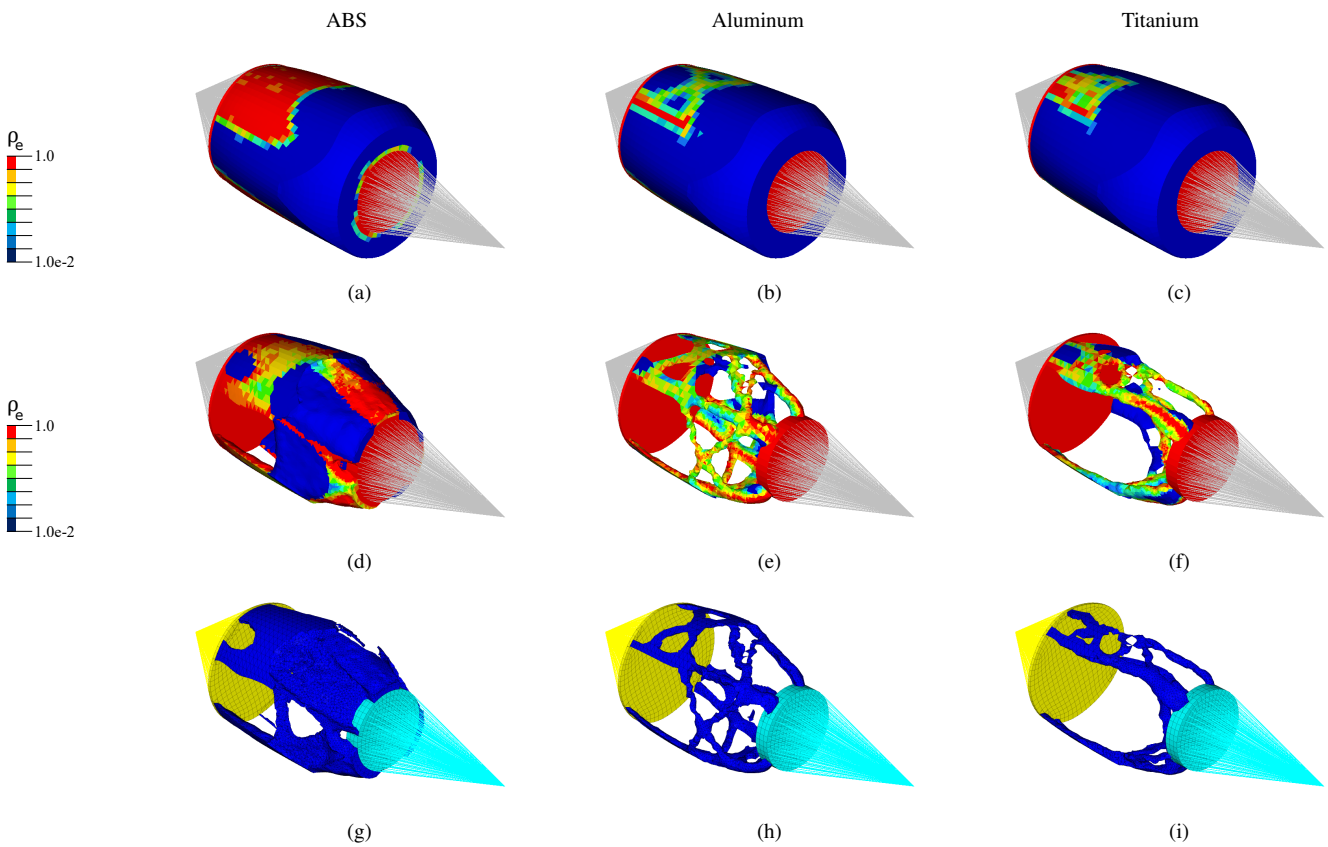

Fig. 7: Topology optimization results of the upper arm: for the first run (a-c), the second run (d-f) and the geometrical interpretation with a threshold $\rho_{th} = 0.5$ (g-i)

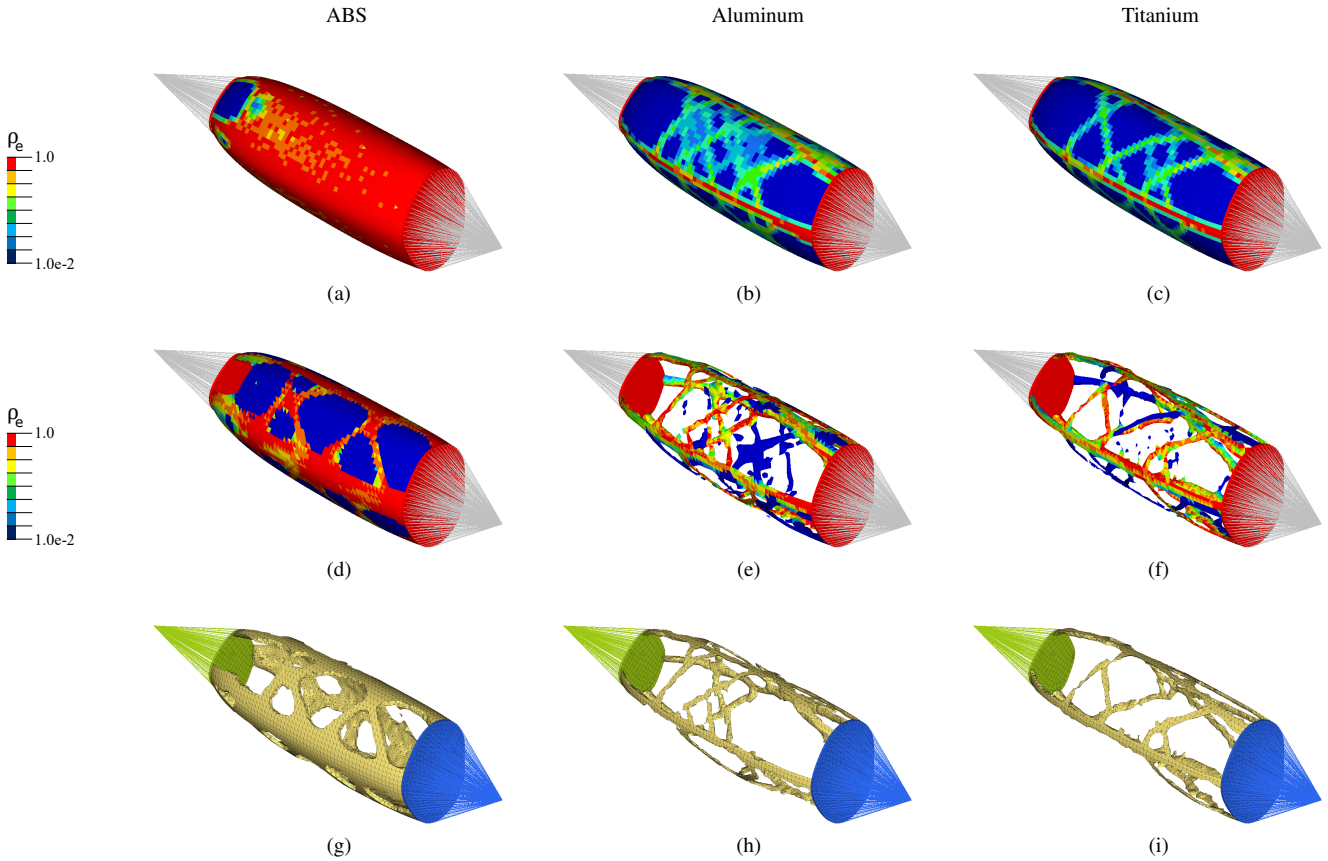

Fig. 8: Topology optimization results of the lower arm: for the first run (a-c), the second run (d-f) and the geometrical interpretation with a threshold $\rho_{th} = 0.5$ (g-i)

five different load cases (cf. Eq. (10) and (11)), only one stiffness matrix inversion per component material combination was necessary. As one drawback of the presented approach, the resulting topologies depend on the stiffness budget distribution α assigned to the components. Therefore, it cannot be ensured that final design is close to the global optimum of the monolithic system optimization.

VI. Conclusion

The overall objective was to design a lightweight, additive manufactured two-segment robot arm. Two system requirements with respect to the end effector deflection and the geometric design domain were formulated. From the displacement requirement five representative static load cases were derived. In order to reduce the computational costs, a modular design approach was presented. Requirements for the lower and upper arm could were derived by allocating stiffness budgets to each component. They were subsequently used to carry out independent topology optimizations. Three different materials were investigated, where the aluminum concept proved to be the lightest choice for lower and upper arm. The results for titanium showed slightly heavier designs, whereas ABS resulted in the heaviest structure for both segments.

In conclusion, the decoupling procedure could reduce the computational time significantly, because not only the combinatorics of the utilized materials but also multiple static load cases could be treated with one matrix inversion. The result of the applied optimization scheme produced three designs for each segments and in total nine concepts for a lightweight robot arm that all satisfy the given system requirements.

For future work, the transfer of the topology optimization results to a physical structure is to be included in the design process. Therefore, a reliable procedure that ensures mass optimality also for the manufactured structure is needed. Also, an improved allocation method for the stiffness budget distribution may improve the results. This could be done for instance by regression models that predict a mass beneficial distribution ratio. As for now, displacement constraints were utilized, a requirement formulation based on stiffness matrices could further increase the information density of the component descriptions. Finally, dynamic load cases should be included to the methodology, as well.

Appendix
Motivation of stiffness budget distribution

For the motivation of a meaningful stiffness budget distribution α for two components, the realized stiffness distribution of an optimal structure is analyzed. Consider a theoretical cantilever i-beam (also known as H-beam) with varying flange width $b(x)$ and negligible web width. It is clamped on one end, i.e., $w(0) = w'(0) = 0$, and subject to a vertical load F on the other end at $x{=}l$. From Bernoulli beam theory follows that $EI(x)w''(x) = F(l-x)$ with Young's modulus E, the moment of inertia $I(x) = b(x)\ h^2\ t/2$, beam length l, flange thickness t and profile height h. The beam deflection at position x reads $w(x) = \int_0^x d\xi \frac{F(l-\xi)(x-\xi)}{EI(\xi)}$. For similarity to the main design problem, assume that the profile height is constraint to a constant value of h, and minimize the mass subject to a displacement constraint:

$$\begin{aligned} &\min_{b(x)} m_{cb}(b(x)) \\ &\text{s. t.:} \quad w(l) \leq d_0. \end{aligned} \tag{12}$$

The optimal distribution of $b(x)$ is obtained by variation of the Lagrangian function

$$L(b(x)) = \int_0^l 2\rho t b(x) dx + \lambda \left[\int_0^l \frac{2(l-x)^2}{Eh^2 t b(x)} dx – d_0 \right] \tag{13}$$

with respect to $b(x)$, where λ is the Lagrange multiplier associated with the displacement constraint. The resulting solution $b(x) = \frac{Fl^3}{Eh^2 t d_0}(1-x/l)$ with deflection $w(x) = d_0 x^2/l^2$ has the stiffness distribution

$$\frac{w(l/2) + (l/2)w'(l/2)}{w(l)} = 3/4, \tag{14}$$

where the intervals $[0, l/2]$ and $[l/2, l]$ are interpreted as components 1 and 2, respectively.

References

[1] A. Albu-Schäffer, S. Haddadin, C. Ott, A. Stemmer, T. Wimböck, and G. Hirzinger, "The dlr lightweight robot: Design and control concepts for robots in human environments," *Industrial Robot: An International Journal*, vol. 34, no. 5, pp. 376–385, 2007.

[2] D. Buchler, H. Ott, and J. Peters, "A lightweight robotic arm with pneumatic muscles for robot learning," in *2016 IEEE International Conference on Robotics and Automation, Stockholm, Sweden, May 16th-21st*, A. Okamura and A. Menciassi, Eds. Piscataway, NJ: IEEE, 2016, pp. 4086–4092.

[3] S. Mori, K. Tanaka, S. Nishikawa, R. Niiyama, and Y. Kuniyoshi, "High-speed and lightweight humanoid robot arm for a skillful badminton robot," *IEEE Robotics and Automation Letters*, vol. 3, no. 3, pp. 1727–1734, 2018.

[4] M. P. Bendsøe and O. Sigmund, *Topology Optimization: Theory, Methods, and Applications*, second edition, corrected printing ed. Berlin and Heidelberg: Springer, 2004. [Online]. Available: http://dx.doi.org/10.1007/978-3-662-05086-6

[5] A. Albers, S. Brudniok, J. Ottnad, C. Sauter, and K. Sedchaicharn, "Upper body of a new humanoid robot - the design of armar iii," in *Leg Design for a Humanoid Walking Robot*, Sebastian Lohmeier, Ed. Piscataway, NJ: IEEE Operations Center, 2005, pp. 308–313.

[6] W. Kwon, H. K. Kim, J. K. Park, C. H. Roh, J. Lee, J. Park, W.-K. Kim, and K. Roh, "Biped humanoid robot mahru iii," in *7th IEEE-RAS International Conference on Humanoid Robots, 2007.* Piscataway, NJ: IEEE, 2007, pp. 583–588.

[7] S. Junk, B. Klerch, L. Nasdala, and U. Hochberg, "Topology optimization for additive manufacturing using a component of a humanoid robot," *Procedia CIRP*, vol. 70, pp. 102–107, 2018.

[8] H. B. Huang and G. Zhang, "The topology optimization for l-shape arm of motorman-hp20 robot," *Applied Mechanics and Materials*, vol. 201-202, pp. 871–874, 2012.

[9] Yunfei B., Ming C., Yongyao L., "Structural topology optimization for a robot upper arm based on simp method," *Ding X., Kong X., Dai J. (eds) Advances in Reconfigurable Mechanisms and Robots II. Mechanisms and Machine Science,, vol 36. Springer, Cham.*, 2015.

[10] J. R. R. A. Martins and A. B. Lambe, "Multidisciplinary design optimization: A survey of architectures," *AIAA Journal*, vol. 51, no. 9, pp. 2049–2075, 2013.

[11] Y. Zhou and K. Saitou, "Gradient-based multi-component topology optimization for stamped sheet metal assemblies (mto-s)," *Structural and Multidisciplinary Optimization*, vol. 58, no. 1, pp. 83–94, 2018.
[12] H. M. Kim, N. F. Michelena, P. Y. Papalambros, and T. Jiang, "Target cascading in optimal system design," *Journal of Mechanical Design*, vol. 125, no. 3, pp. 474–480, 2003.
[13] V. Pan, "Complexity of parallel matrix computations," *Theoretical Computer Science*, vol. 54, no. 1, pp. 65–85, 1987.
[14] B. J. Kim, D. K. Yun, S. H. Lee, and G.-W. Jang, "Topology optimization of industrial robots for system-level stiffness maximization by using part-level metamodels," *Structural and Multidisciplinary Optimization*, vol. 54, no. 4, pp. 1061–1071, 2016.
[15] X. Wang, T. Keya, and K. Chou, "Build height effect on the inconel 718 parts fabricated by selective laser melting," *Procedia Manufacturing*, vol. 5, pp. 1006–1017, 2016.
[16] R. L. Huston, "The measure of man and woman – human factors in design alvin r. tilley, henry dreyfuss associates 1993, 96 pages, $60.00 new york: Whitney library of design, watson-guptill isbn 0-8230-3031-8," *Ergonomics in Design: The Quarterly of Human Factors Applications*, vol. 2, no. 2, pp. 37–39, 1994.
[17] M. Zimmermann, S. Königs, C. Niemeyer, J. Fender, C. Zeherbauer, R. Vitale, and M. Wahle, "On the design of large systems subject to uncertainty," *Journal of Engineering Design*, vol. 28, no. 4, pp. 233–254, 2017.
[18] M. Zimmermann and J. E. von Hoessle, "Computing solution spaces for robust design," *International Journal for Numerical Methods in Engineering*, vol. 94, no. 3, pp. 290–307, 2013.
[19] M. Daub, F. Duddeck, and M. Zimmermann, "Optimizing component solution spaces for systems design," *Structural and Multidisciplinary Optimization*, vol. 61, no. 5, pp. 2097–2109, 2020.
[20] T. Rodriguez, M. Montemurro, P. Le Texier, and J. Pailhès, "Structural displacement requirement in a topology optimization algorithm based on isogeometric entities," *Journal of Optimization Theory and Applications*, vol. 184, no. 1, pp. 250–276, 2020.